



# New insights into microstructure evolution mechanism of compacted loess and its engineering implications

Panpan Xu<sup>1,2</sup> · Hui Qian<sup>1,2</sup> · Jie Chen<sup>1,2</sup> · Lingbo Wang<sup>1,2</sup> · Xayda Abliz<sup>1,2</sup> · Xiaoqiang He<sup>1,2</sup> · Gaoxiang Ma<sup>1,2</sup> · Yuan Liu<sup>1,2</sup>

Received: 28 April 2022 / Accepted: 27 December 2022 / Published online: 5 January 2023  
© Springer-Verlag GmbH Germany, part of Springer Nature 2023

## Abstract

As the macroscopic mechanical properties of soil are closely related to its microstructure, and loess historically played an important role in engineering construction, the effect of compaction on the microstructure of compacted loess was investigated using scanning electron microscopy (SEM) and mercury intrusion porosimetry (MIP) in this study. The SEM imaging results showed that as compaction degree increased, the loess microstructure evolved from an overhead weak into an interlocking semi-cementation, and then into a dispersion-strong cementation. Correspondingly, the pore characteristics mainly exhibited a transformation from macropores (diameter > 32  $\mu\text{m}$ ) to mesopores (diameter between 8 and 32  $\mu\text{m}$ ) and then to small pores (diameter between 2 and 8  $\mu\text{m}$ ). The MIP test results showed that the content volume of intragranular pores (diameter between 1.8 and 70  $\mu\text{m}$ ) decreased with increasing loess compactness, whereas the contents of intra-particle, interparticle, and intergranular pores were stable, indicating that the compaction of loess was mainly caused by compression of the intragranular pores. Additionally, the variation interval of the dominant pore type (intragranular pore) observed by the MIP test was consistent with the comprehensive variation interval of the pore types (macropore, mesopore, and small pores) observed by SEM imagery. These findings are helpful to explain the linkage law between loess structure, engineering characteristics, and catastrophic effects.

**Keywords** Microstructure evolution · Compacted loess · Engineering implications · SEM imagery · MIP test

## Introduction

Loess and loess-like soils are widely distributed globally, accounting for approximately 10% of the terrestrial surface (Li et al. 2018; Pécsi 1990; Xu et al. 2020b). China has the widest loess distribution, especially in the northwest, which forms the Chinese Loess Plateau (Derbyshire 2001; Li 2018; Luo et al. 2018). Loess has been used as a basic material in various engineering constructions since ancient times; it was used in the Great Wall and the Daming Palace, as well as in more recent projects such as those of “moving mountains and building cities” and “harnessing gully and making land”

(Li et al. 2014; Xu et al. 2021e). In addition, loess structures widely distributed in northwest China play an irreplaceable role in people’s life and agricultural economic development (Xu 2021). Thus, loess is an essential material in engineering applications. However, the engineering performance of loess reduces over time as the mechanical properties of soil change irreversibly because of factors such as loess properties, extreme climate, and other natural factors as well as increasing human engineering activities (Assadi-Langroudi et al. 2018; Li 2018; Qi and Vanapalli 2015; Wang et al. 2019; Xu et al. 2020a). The above phenomenon is attributed to damage to the microstructure of soil due to multiple factors. Therefore, investigating the evolution characteristics and formation mechanism of compacted loess microstructure will provide basic data for explaining loess macro-mechanical behavior, which has greatly theoretical significance. Meanwhile, it can also present certain guidelines for engineering constructions such as deep compacted highways, earth rock dams, and high-fill foundations in loess areas, and has importantly practical significance.

✉ Hui Qian  
qianhui@chd.edu.cn

<sup>1</sup> School of Water and Environment, Chang’an University, Xi’an 710054, Shaanxi, China

<sup>2</sup> Key Laboratory of Subsurface Hydrology and Ecological Effects in Arid Region of the Ministry of Education, Chang’an University, Xi’an 710054, Shaanxi, China

For interpreting macroscopic behavior, microstructure refers to the size, shape, and arrangement of particles and pores, as well as the cementation degree and structural connection mode of each unit (Li et al. 2019; Munoz-Castelblanco et al. 2012; Rabot et al. 2018). Presently, advanced methodologies for characterizing soil microstructure can be divided into two categories: direct and indirect methods. The direct method mainly includes optical microscopy (OM), scanning electron microscopy (SEM), and X-ray computed tomography (CT); the indirect method mainly includes mercury intrusion porosimetry (MIP) and gas adsorption method (GAM) (Rabot et al. 2018). SEM, as one of the direct methods to investigate soil microstructure, is mostly used in research because of its simple sample preparation, high resolution, and qualitative and quantitative analyses (Xu et al. 2021c). Several valuable findings have emerged from the application of SEM imaging technology. By using SEM, Jiang et al. (2014) explored the mechanism of microstructure changes of intact and remolded loess caused by loading. Liu et al. (2015) performed SEM tests and proposed a conceptual model of loess microstructure, which can characterize morphology properties and explain changes in collapsibility. Luo et al. (2018) examined triaxial and uniaxial compression tests and SEM tests of undisturbed loess under humidification conditions and found that the structure of surface loess is mainly metastable, whereas the structure of bottom loess is mainly affected by intergranular cementation. By using SEM imagery, Xu et al. (2021a) explored the anisotropic microstructure of loess and paleosol, their differences and similarities, and the significance in engineering construction and paleoenvironment. Additionally, SEM can quantitatively distinguish pores and particles through image processing technology (e.g., the Image-Pro Plus software); it can also describe pore and particle number, size, and morphology (Hou et al. 2021; Xu et al. 2021c).

MIP is a common method for characterizing pore size distribution (PSD) because of its simple principle and wide test range of 0.003–1000  $\mu\text{m}$  (Giesche 2006; Zhang et al. 2018). The MIP method has been applied successfully in several studies to investigate the PSD of soil and achieved a series of meaningful findings (Jozefaciuk et al. 2015; Nan et al. 2021; Wang et al. 2020a; Zhang et al. 2019). Zhang et al. (2019) reported the influence mechanism of compaction on the microstructure of micro-expansive remolded mudstone through MIP testing. Wang et al. (2020a) also characterized the distribution of micropores of remolded loess through the MIP test, and they noted that soil seepage at a low hydraulic gradient is a non-Darcy flow. Kloubek (1981) and Jozefaciuk et al. (2015) found that the difference between the intrusion and extrusion curves of soil is mainly caused by the ink-bottle effect of pores.

Although SEM and MIP were used to determine the evolution characteristics of soil microstructure, the methods also have their own disadvantages. In the actual operation of MIP, high-pressure mercury injection destroys the original pore structure and affects the test results. In addition, MIP cannot determine particle and pore morphology. Meanwhile, SEM evaluates the microstructure parameters from a two-dimensional perspective, especially the quantitative description, which may alter the analysis results. Therefore, SEM and MIP are typically combined for complementary advantages and for scientifically and reasonably determining the micro-mechanism of changes in the macro-mechanical behavior of soil (Assallay et al. 1996; Ge et al. 2021; Romero 2013; Wang et al. 2019, 2020b). For example, Romero (2013) provided a new insight into the influence of microstructure on the hydraulic properties of compacted clayey soil. Wang et al. (2019) investigated the evolution law of pore size distribution by consolidating undisturbed loess and remolded loess. Furthermore, Ge et al. (2021) combined SEM and MIP to evaluate the effect of soil microstructure wetting-induced collapse on compacted loess. These studies indicate that the comparison and combination of SEM and MIP can improve the reliability of studies on soil microstructure mechanism. Although the research in this field has made well-known progress, there are still the following shortcomings: (1) the understanding of the four key elements (skeleton particle shape, contact relationship, pore type, and cementation degree) of compacted loess microstructure in the qualitative description of SEM is not systematic, (2) a wealth of discoveries has been obtained based on the combination of qualitative description of SEM and quantitative analysis of MIP, rarely involving the comprehensive consideration of quantitative analysis of SEM, and (3) there is a lack of consistency analysis and discussion on the evaluation results of the pore classification and size of compacted loess using SEM and MIP.

Loess is a special engineering soil with characteristics of under-compaction, collapsibility, water sensitivity, and disintegration. To meet different requirements in engineering practice, loess compactness is often changed through compaction to form remolded loess with different compaction degrees. Compaction degree (a common and prominent index for characterizing soil structure) is a vital factor of compacted soil engineering performance, and its acquisition does not require special technology or expensive equipment (Rabot et al. 2018). This paper used SEM and MIP test methods and advanced image processing technology IPP to explore the microstructure characteristics of compacted loess with six compaction degrees, to clarify the formation and evolution mechanism of compacted loess microstructure, and to determine the consistency of SEM and MIP evaluation results on microstructure.

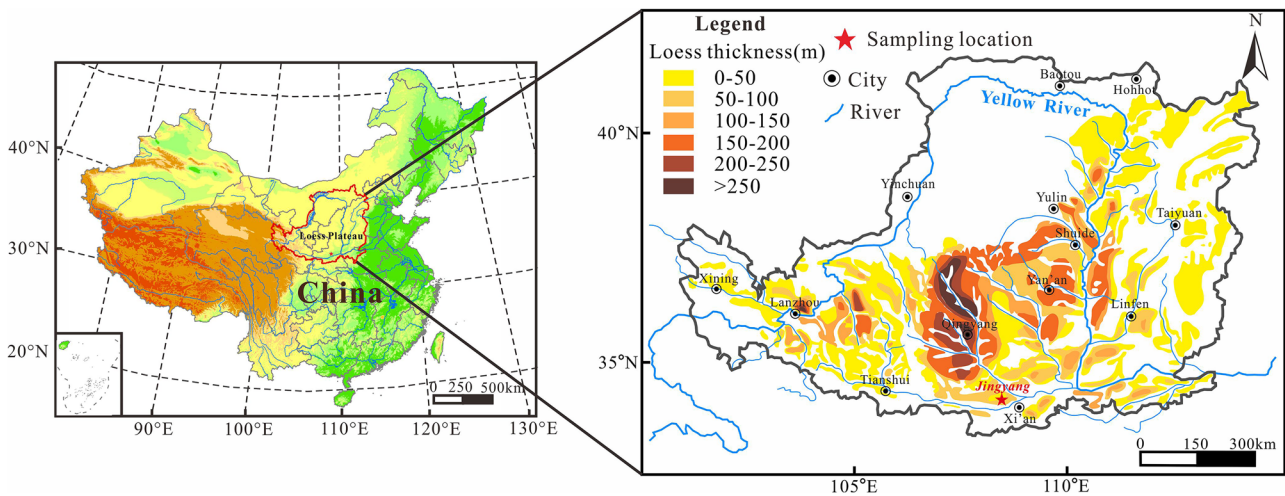


Fig. 1 Spatial distribution of Chinese Loess Plateau and location of sampling site (modified from Wang et al. 2010)

## Materials and methods

### Test material

Malan loess in southern Chinese Loess Plateau was collected as the test material (Fig. 1). Its basic physical properties including maximum dry density, optimal moisture content, specific gravity, as well as liquid limit and plastic limit, were measured according to Standard for Geotechnical Testing Method (SGTM 2019); the test results are presented in Table 1. The particle size distribution of loess was obtained using a WJL-602 laser particle size analyzer, and it is composed of 13.21% silt, 86.63% clay, and 0.16% sand according to the classification system of US Department of Agriculture (USDA 1951) (Table 1). The uniformity coefficient (9.70) and the coefficient of gradation of loess particles (1.58) were obtained by calculation (Wang and Qiu 2017), which indicated that the loess was of good grade and could achieve high compactness through compaction. The loess is a low-plasticity clay (CL) according to the United Soil Classification System (ASTM 2006).

### Sample preparation

The loess collected in the field was pulverized using a rubber mallet, air dried, and passed through a 2-mm sieve. The

required amount of deionized water was evenly mixed in the loess at 105 °C for 8 h, to reach the optimum moisture content of 17%. The wet soil was sealed in a plastic bag to equilibrate for 24 h prior to compaction. Subsequently, the compacted loess samples (6.18 cm diameter and 4 cm height) were prepared using a triaxial compaction apparatus. Samples with six dry densities, i.e., 1.30, 1.35, 1.40, 1.45, 1.55, and 1.65 g·cm<sup>-3</sup>, were designed and produced to investigate the evolution characteristics and mechanism of compacted loess microstructure. The corresponding compaction degrees were obtained using Eq. (1), as shown in Table 2:

$$D_c = \frac{\rho_d}{\rho_{dmax}} \times 100\% \tag{1}$$

where  $D_c$  is compaction degree (%),  $\rho_d$  is dry density (g/cm<sup>3</sup>), and  $\rho_{dmax}$  is maximum dry density of loess obtained from an indoor compaction test.

### SEM tests

#### Sample preparation and observation

The soil sub-samples (small soil columns) were obtained from the center of the compacted loess samples and air dried, because this drying method is simple, economical, and has little disturbance to the sample structure.

Table 1 Physical properties of Malan loess

Maximum dry density ( $\rho_{dmax}$ )/g·cm <sup>-3</sup>	Optimal moisture content ( $\omega_{opt}$ )/%	Specific gravity ( $G_s$ )	Liquid limit ( $W_L$ )/%	Plastic limit ( $W_p$ )/%	Particle size distribution /%		
					Clay (< 2 μm)	Silt (2–50 μm)	Sand (50–2000 μm)
1.74	17.07	2.71	34.5	20.1	13.21	86.63	0.16

**Table 2** Test design of compacted loess samples

Dry density/g·cm <sup>-3</sup>	1.30	1.35	1.40	1.45	1.55	1.65
Compaction degree/%	74.71	77.59	80.46	83.33	89.08	94.83

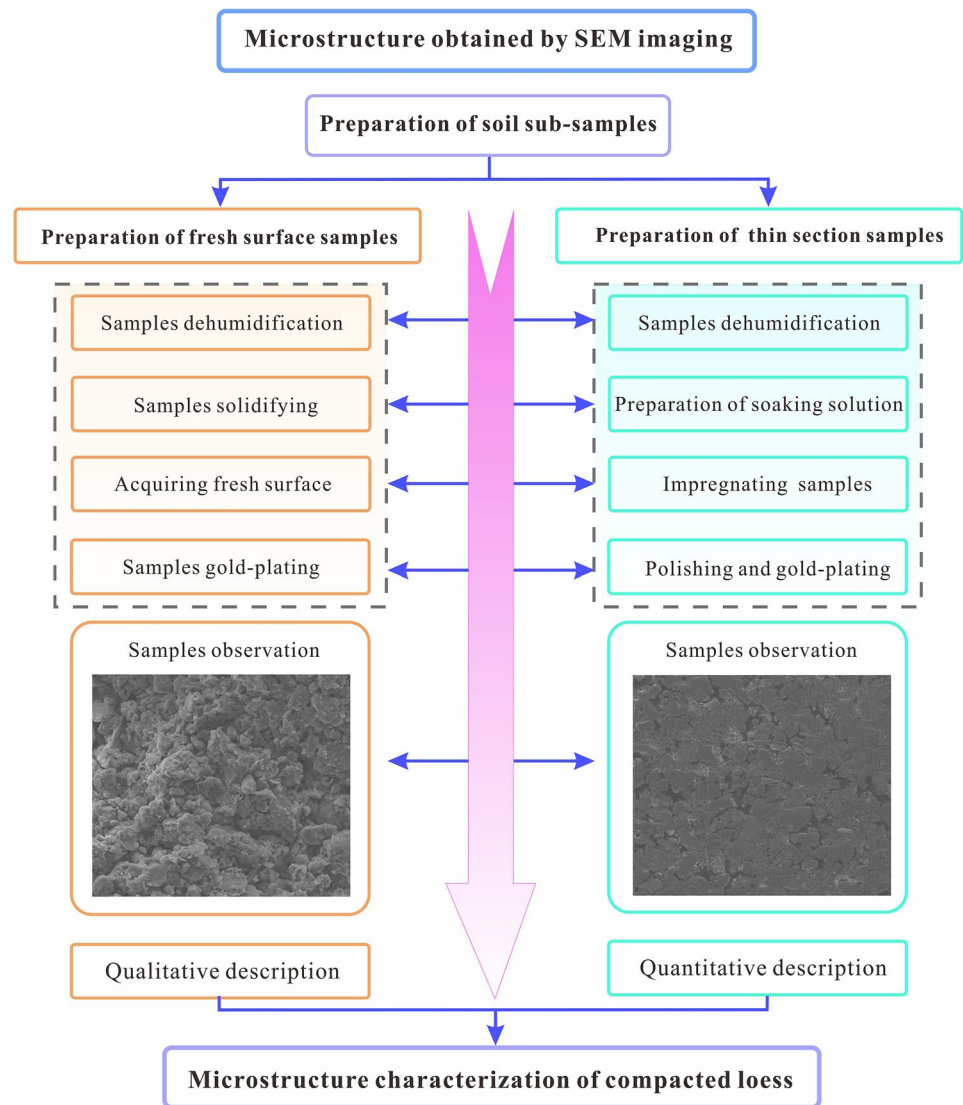
Subsequently, fresh surface samples and thin sections were prepared. The corresponding procedure is illustrated in Fig. 2. In the gold-plating step, all the samples were coated using an SCD-005 ion sputtering instrument. In the next observation step, image acquisition was performed using a scanning electron microscope (FEI Quanta 200). When the loess microstructure is magnified 1000–4000 times, the four key elements of skeleton particle shape, contact relationship, pore type, and cementation degree can be clearly identified (Xu 2021). Meanwhile, considering that the larger scope of soil samples can be observed, two-dimensional images with 2000-fold magnification of fresh surface samples adequately and qualitatively reflect

the morphology of the microstructure (Hou et al. 2021). As for SEM quantitative description, the magnified 500–1000X image is suitable for obtaining and analyzing pore parameters (Xu 2021). Li and Li (2017) also reported that 800-fold is an ideal choice for a reasonable observation field and accurate results. Therefore, 2000X and 800X magnifications were selected for qualitative and quantitative investigations of loess microstructure, respectively.

**Image processing**

For image processing and data acquisition, we used Image-Pro Plus 6.0 (IPP 6.0), which has been widely used for obtaining

**Fig. 2** Procedure for the microstructure analysis by SEM imaging technology (modified from Hou et al. 2021; Xu et al. 2021a)





quantitative information of soil microstructure (Delage and Lefebvre 1984; Li and Li 2017; Xu et al. 2021c). The original image of the microstructure is shown in Fig. 3a. As Li and Li (2017) and Xu (2021) described, the binary image was obtained after the image processing of contrast enhancement, noise reduction, and segmentation (Fig. 3b). The black and white areas represent pores and particle skeleton, respectively. According to Lei’s classification standard for pores in loess (Lei 1987), pores can be divided into four categories (Fig. 3c): red, cyan, green, and blue areas, representing micropores, small pores, mesopores, and macropores, respectively, with corresponding pore diameters < 2, 2–8, 8–32, and > 32 μm. It is worth emphasizing that pore diameter is the average length of diameters measured at 2-degree intervals and passing through pore’s centroid using IPP 6.0, and its calculation formula is as follows:

$$D_{\text{pore}} = \frac{\sum_{i=1}^J d_i}{J} \tag{2}$$

where  $D_{\text{pore}}$  is pore diameter (μm),  $d_i$  is the measured value of pore diameter in each 2-degree interval (μm), and  $J$  is the amount of measured values (Xu et al. 2021a).

**MIP test**

MIP is an effective technique for characterizing soil microstructure (Ge et al. 2021; Ng et al. 2016; Romero 2013; Wang et al. 2020b). Prior to MIP testing, the soil samples shall be uniformly pretreated in strict accordance with the procedures, including the preparation and dehydration of compacted loess samples (Wang et al. 2020a; Xu et al. 2022a). The external loess samples are easily disturbed, and the inconsistent sampling positions are also easy to result in test errors. Furthermore, considering the maximum volume of soil sample that can be accommodated in

the test instrument, the cubes (10 mm) were acquired from the center of the compacted loess samples to improve the accuracy of the test and the reliability of the results as much as possible. The MIP test principle is to connect the applied pressure ( $p$ ) of a non-wetting liquid (mercury) with pore diameter ( $d$ ) using Eq. (3) (Washburn 1921):

$$p = -\frac{4\sigma_{\text{Hg}} \cos(\theta)}{d} \tag{3}$$

where  $\sigma_{\text{Hg}}$  is the surface tension of mercury (0.484 N/m) and  $\theta$  is the contact angle between mercury and the pore wall, which is recommended as 130° (Monroy et al. 2010; Xu et al. 2021b). In this work, an Autopore IV 9500 mercury intrusion porosimeter was used to measure the pore size of compacted loess.

**Permeability test**

The quantitative characteristics of water flow in porous media are usually obtained by Darcy’s law (Daniel 1994). However, factors that significantly affect permeability, such as soil structure, mineral composition, and fluid properties, make this law less applicable for clayey soils with low permeability (Alabi 2011; Al-Taie et al. 2014; Hansbo 2001). The loess used in this study belongs to the clayey type. Zhang et al. (2016) and Zhang et al. (2013) also reported that loess had low permeability. When the hydraulic gradient is not less than 3, the velocity of compacted loess with a dry density of 1.20–1.80 g/cm<sup>3</sup> shows a good positive correlation with the hydraulic gradient, i.e., it is consistent with the Darcy seepage characteristics (Wang et al. 2020a). Considering the damage of high hydraulic gradient to loess structure, the hydraulic gradient was set to 3 in this study. The TST-55 permeameter was used to measure the  $K_{\text{sat}}$  of the compacted loess samples (6.18 cm diameter and 4 cm height) using the constant head method, which has been

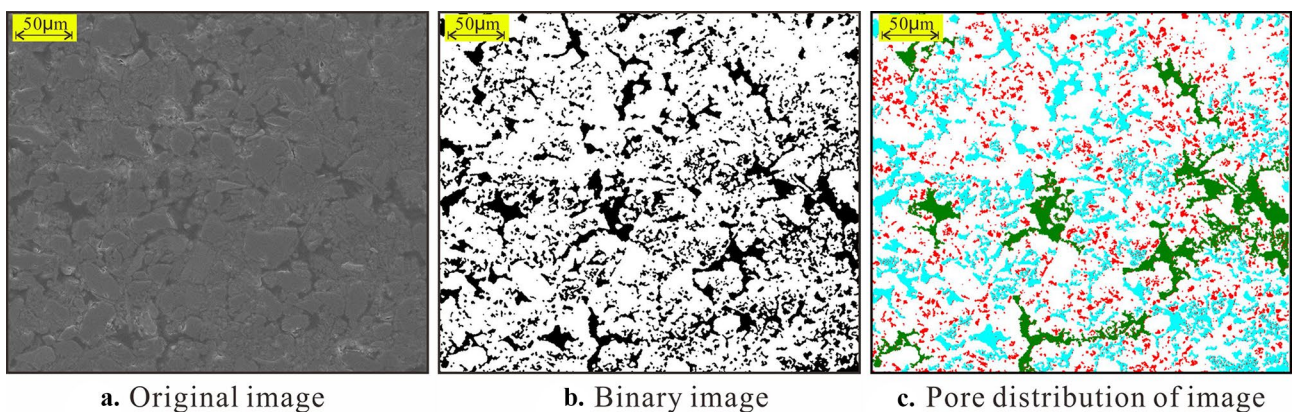


**Fig. 3** Image post-processing for quantitative analysis of pores

widely used to study the permeability of saturated soil (Ali et al. 2019; Bourazanis et al. 2016; Wang et al. 2020a). The calculation formula is as follows:

$$K_{\text{sat}} = \frac{Q \cdot L}{A \cdot t \cdot \Delta h} \quad (4)$$

where  $K_{\text{sat}}$  is the saturated hydraulic conductivity (cm/s),  $Q$  is the amount of water overflow (cm<sup>3</sup>),  $A$  is the cross-sectional area of the sample (cm<sup>2</sup>),  $t$  is the time (s) required for  $Q$  to be discharged,  $\Delta h$  is the hydraulic head drop across the soil sample (cm),  $L$  is the length of seepage path (i.e., height of sample) (cm), and  $\Delta h/L$  is the hydraulic gradient (dimensionless). In the saturated permeability test of the Standard for Geotechnical Test Methods (SGTM 2019), 20 °C was specified as the standard temperature. Therefore, the temperature of this test environment was controlled at 20 °C to avoid correction of the  $K_{\text{sat}}$  of the compacted loess. The permeability cycle was set to 7 days, and data were recorded at approximately 12-h intervals (Xu et al. 2020a).

## Results

### Evolution of microstructural morphology

The microstructure of loess is typically described by four key elements: skeleton particle shape, contact relationship, pore type, and cementation degree. These elements are interdependent and widely used in studying loess engineering properties (Li et al. 2016, 2019; Xie et al. 2018; Xu et al. 2021a; Xu 2021). Additionally, according to these four elements, the structure of loess can be categorized into overhead, interlocking, and matrix structures (Fig. 4) (Xu et al. 2021c). In Fig. 4a, the contact area between soil particles is small, resulting in the connection mode being mainly point contact with weak cementation, which can also be understood as overhead contact between particles, forming overhead pores. This loess structure has strong permeability, but it is extremely unstable and prone to collapse. In Fig. 4b, the particles are stacked together by interlocking, which

contributes to the increase of the contact area and cementation degree. The contact mode of particles coexists with face contact and point contact, forming interlocking pores. The structure is relatively stable with good permeability and is generally not easy to collapse. In Fig. 4c, the particles are closely arranged, and the pores are basically filled with cement or debris, with a high degree of cementation. Its structure is stable and almost no collapsible deformation occurs; meanwhile, the pore connectivity of soil is poor, leading to the weak permeability.

The microstructural morphology of loess samples under varying compactness is shown in Fig. 5. The natural loess has undergone the pretreatment procedure as shown in “Sample preparation” section, which ensures that the particle size of the loess sample has a consistent range (Liet al. 2022; Yan et al. 2021). The loess particle aggregates are formed between the particle units by the attractive force after water spraying, and the larger the particle size, the weaker the soil strength and the worse the stability. The compaction degree of the loess samples increased because the large-scale aggregates were crushed into small-scale aggregates after compression and deformation to fill the pores and increase the compactness of soil. Based on the four key elements mentioned above, the microstructure characteristics of compacted loess samples are summarized and presented in Table 3. When compactness increased, large-scale soil aggregates were decomposed into small-scale aggregates, filling the pore space by interlocking, cementing with clastic particles, and blurring the skeleton particle outline. As shown in Fig. 5, the particle aggregates of compacted loess samples with dry densities of 1.30 and 1.35 g/cm<sup>3</sup> are large in size, while the contact area between particles is small, forming the contact mode dominated by overhead contact. The soil structure is loose with weak cementation, and the corresponding structure type is shown in Fig. 4a. The large-scale particle aggregates of 1.40, 1.45, and 1.55 g/cm<sup>3</sup> loess samples are broken into small-scale ones under the compaction, the contact pattern of particles gradually changes from point contact to face contact, and the corresponding soil structure gradually changes from the overhead structure in Fig. 4a to the interlocking structure in

**Fig. 4** Conceptual model diagram of loess microstructure

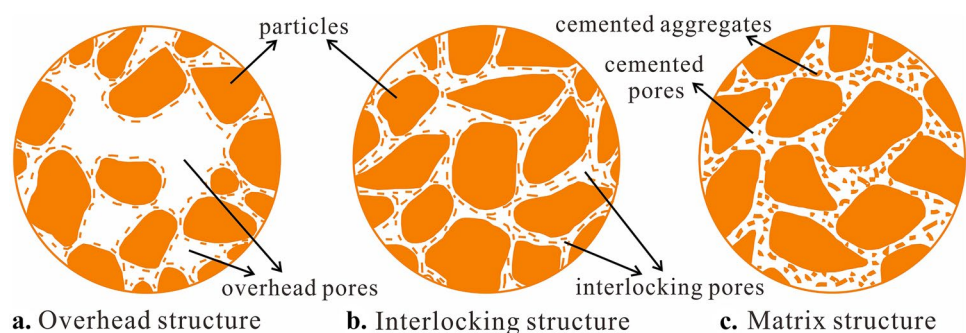


**Fig. 5** SEM images of the microstructural morphology of compacted loess

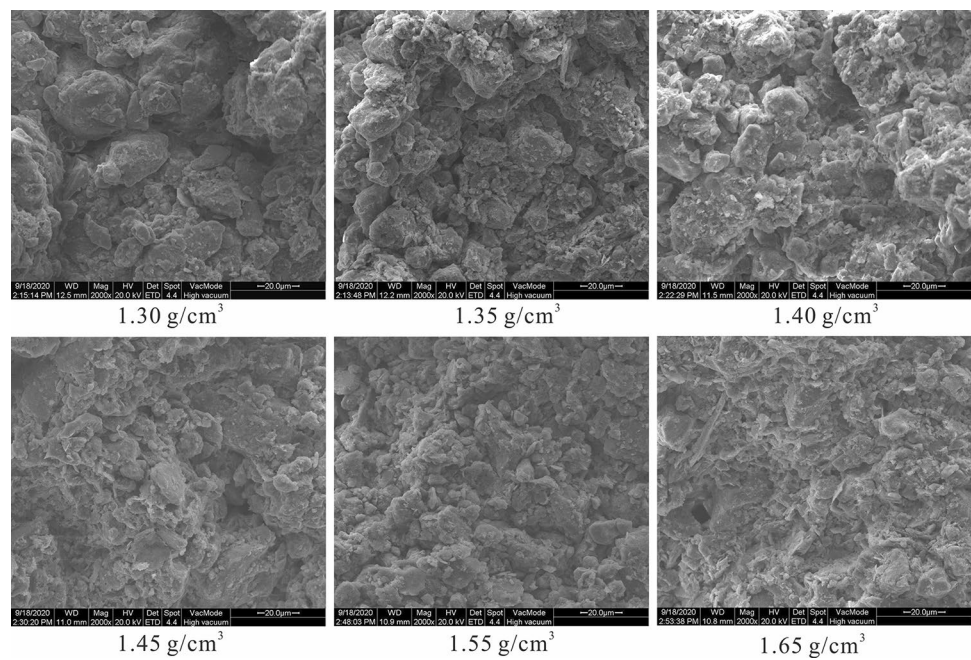


Fig. 4b. As for the 1.65 g/cm<sup>3</sup> loess sample, its soil structure is like the matrix structure shown in Fig. 4c, which is mainly because the aggregate cannot be further broken when the soil is compacted to a certain extent, and the soil structure can only be made denser by flocculating with debris particles (Ma 2017).

In general, in the process of increasing loess compactness, the contact relationship of particles changed from overhead to interlocking and later to dispersion. The pore type also changed from overhead to interlocking and later to cemented pore. The degree of cementation changed from weak cementation to semi cementation and later to strong cementation. The corresponding microstructure evolved from overhead to interlocking and matrix type.

**Pore area distribution**

The SEM images of the thin-section samples were processed using the IPP 6.0 software to obtain the binary images as shown in Fig. 6a, where the white and black areas represent the particle skeleton and pores, respectively. The pore distribution area of compacted loess samples decreased noticeably as dry density (compaction degree) increased. The process of increasing compactness was the process of compressing skeleton particles and filling pore space. According to Lei’s standard (Lei 1987), the distribution of four types of pores in compacted loess is shown in Fig. 6b, and the corresponding pore area is shown in Fig. 7. The content of the total pore area of the loess samples decreased considerably as

**Table 3** Morphological characteristics of soil microstructure

Dry density /g·cm <sup>-3</sup>	Morphological characteristics of soil microstructure				
	Particle shape	Contact relationship	Pore type	Cementation degree	Microstructure type
1.30	Large aggregate particles with almost no clastic particles	Overhead	Overhead pores	Weak cementation	Overhead structure
1.35	Large aggregate particles with trace clastic particles	Overhead	Overhead pores	Weak cementation	Overhead structure
1.40	Large aggregate particles with a few clastic particles	Overhead	Overhead pores	Weak cementation	Overhead-interlocking
1.45	Large aggregate particles with a few clastic particles	Interlocking	Interlocking pores	Semi cementation	Interlocking- overhead
1.55	Smaller aggregate particles with more clastic particles	Dispersion	Interlocking pores and cemented pores	Semi cementation	Interlocking
1.65	Agglomeration of small-scale aggregate and clastic particles	Dispersion	Cemented pores	Strong cementation	Matrix



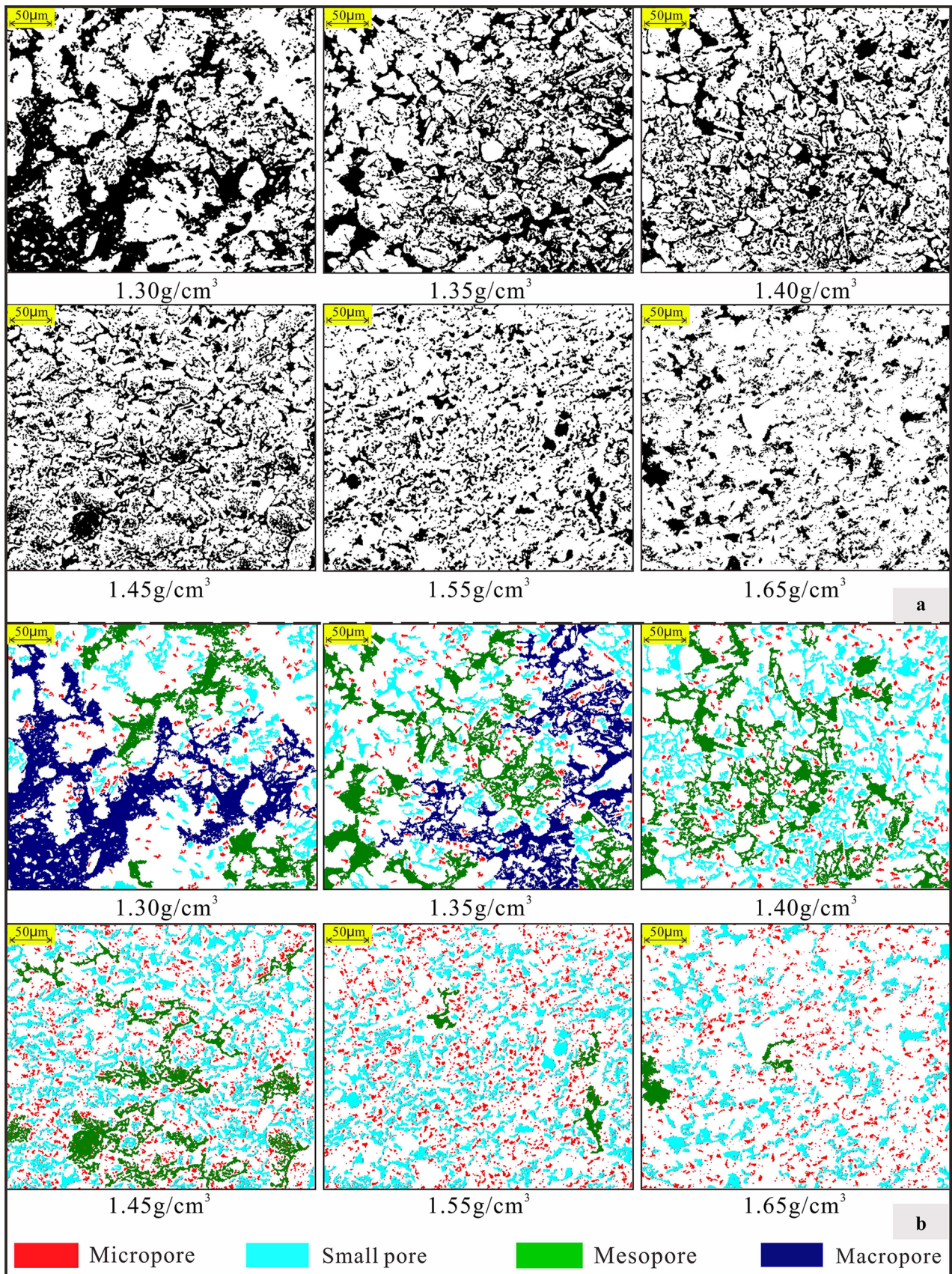
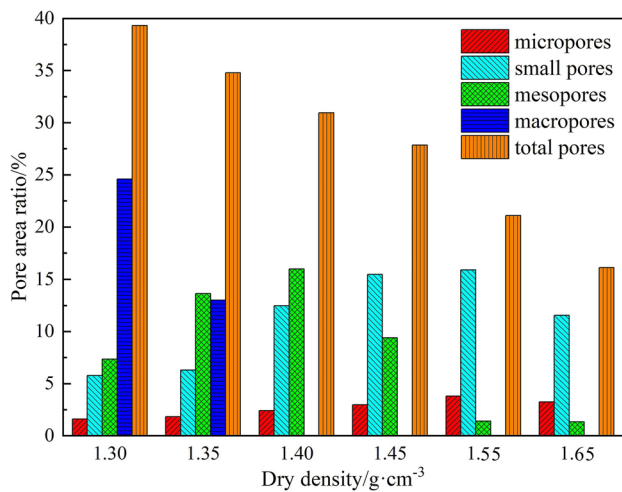


Fig. 6 Pore distribution of specimens: a binary images and b four types of pore distribution (modified from Xu et al. 2021c)





**Fig. 7** Various pore area ratios of compacted loess samples

dry density increased. Only the 1.30 g/cm<sup>3</sup> and 1.35 g/cm<sup>3</sup> samples contained macropores, and the corresponding proportions were 24.59 and 13.01%, respectively. The mesopore area ratios of the 1.40–1.65 g/cm<sup>3</sup> samples were between 1.32 and 15.99%, and the content decreased with increasing compactness. Small pores were the main type of the 1.45, 1.55, and 1.65 g/cm<sup>3</sup> samples, and the micropore content of all the samples slightly changed. It can be observed that increasing the compactness of loess samples mainly caused the transformation from macropores (diameter > 32 μm) to mesopores (diameter between 8 and 32 μm) and then to small pores (diameter between 2 and 8 μm).

**Pore size distribution characteristics**

From the MIP test, the pore size distribution curves of compacted loess specimens under different dry densities were obtained, as shown in Fig. 8, including pore size distribution function and cumulative pore volume. In addition, Shear et al. (1992) classified pores into four categories according to pore diameter: intra-particle pores (diameter < 0.014 μm), interparticle pores (diameter between 0.014 and 1.8 μm), intragranular pores (diameter between 1.8 and 70 μm), and inter-granular pores (diameter > 70 μm). This classification standard has good applicability in pore size characterization based on the MIP test (Shear et al. 1992; Zhang et al. 2019). Therefore, this standard was used for classifying and counting the pores of compacted loess samples. The results are shown in Table 4.

The pore size density curves of compacted loess samples have obvious peaks (Fig. 8a and b). For the 1.30–1.45 g/cm<sup>3</sup> compacted loess samples, the pore size peak (32.82, 24.11, 13.94, and 9.05 μm) decreased as dry density

increased. The pore size peaks of the 1.55 and 1.65 g/cm<sup>3</sup> samples were both 7.24 μm; the distribution density decreased with increase in compaction degree, that is, the peak advantage decreased gradually. Additionally, the pore size density curves showed obvious differences in interval in the intra-granular pores, indicating that the compaction mainly affected this pore type. As shown in Fig. 8c and d, the cumulative pore volume decreased with increase in compactness, that is, from 0.386 to 0.150 mL/g. The curve of the 1.30–1.40 g/cm<sup>3</sup> samples was the steepest in the interval of intragranular pores, and the distribution range decreased as compaction degree increased. The interval of the dominant pore size of 1.45–1.65 g/cm<sup>3</sup> samples became wider, and the curve was steeper in the interval of intragranular and inter-particle pores. This situation suggested that the main pore type in the compacted loess sample was intragranular pores, followed by inter-particle pores.

For pore volume content (presented in Table 4), compaction had a weak effect on the volume content of intra-particle, interparticle, and intergranular pores of the loess samples. The intra-granular pores were substantially reduced. Furthermore, the ratio of various types of pore volumes to the total pore volume is presented in Fig. 9. With the increase in the dry density of compacted loess, the volume ratio of intra-granular pore decreased gradually, whereas the volume ratio of the inter-particle pore increased gradually. For the volume of the other two pore types, the proportion remained unchanged. Meanwhile, the above change in pore volume ratio was mainly due to intra-granular pore reduction. Therefore, the microscopic mechanism of the increase in the macroscopic compactness of loess samples was that intra-granular pore compression caused a transformation from larger pores to smaller pores, resulting in pore space reduction. Zhang et al. (2019) also found that compaction altered the macroscopic physical and mechanical properties of remolded mudstone, which were mainly affected by intra-granular pores.

**Discussion**

**Comparison of pore evaluation**

For a more comprehensive and reasonable comparison of the above pore analysis results based on SEM and MIP, Eq. (5) was used for calculating the theoretical porosity of compacted loess samples (Xu et al. 2021a):

$$n = (1 - \frac{\rho_d}{G_s}) \times 100\% \tag{5}$$

where *n* is theoretical porosity of compacted loess samples,  $\rho_d$  is dry density of samples, and  $G_s$  is specific gravity of loess used in this study. The calculation results are presented in Table 5.

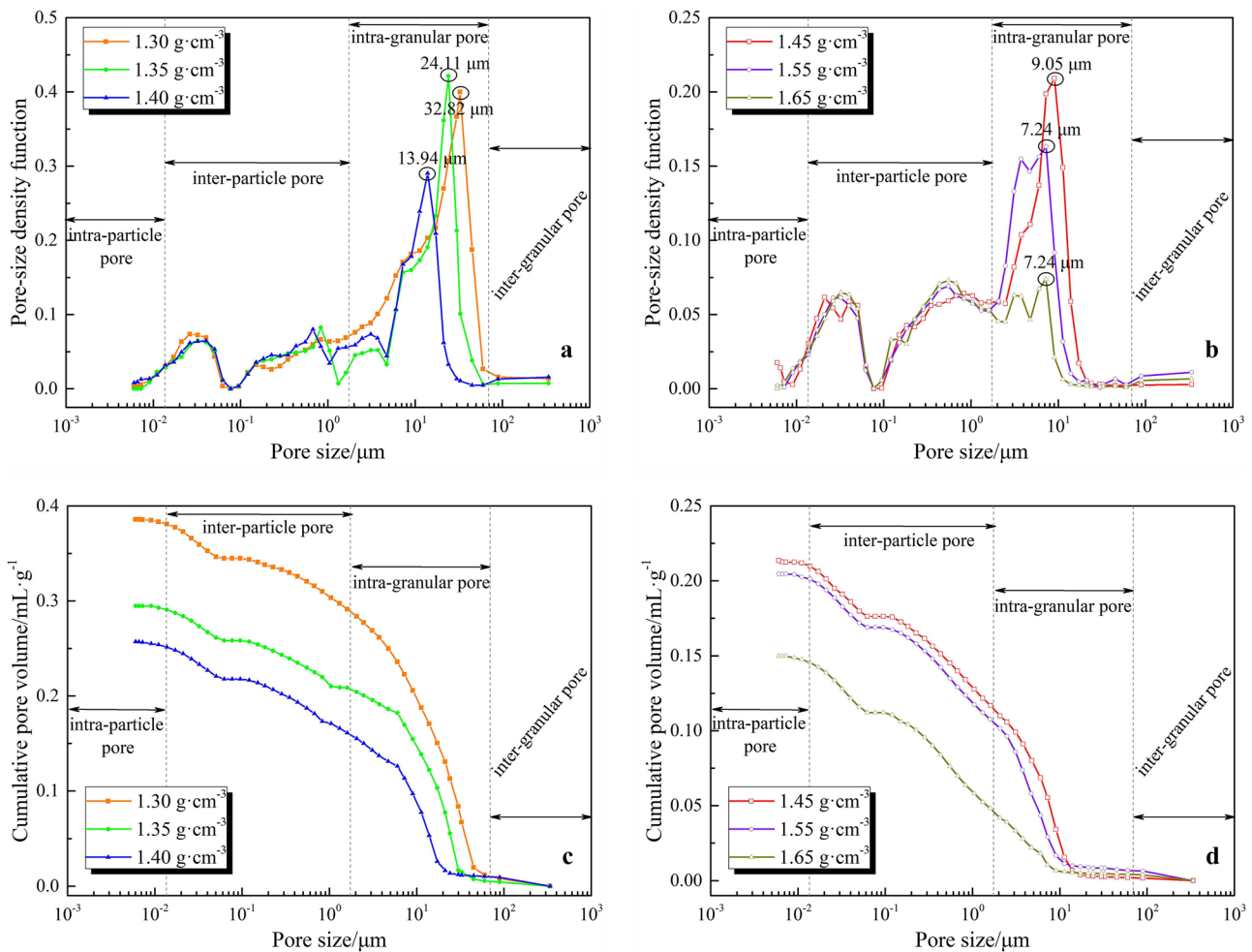


**Fig. 8** Pore size distribution of compacted loess samples

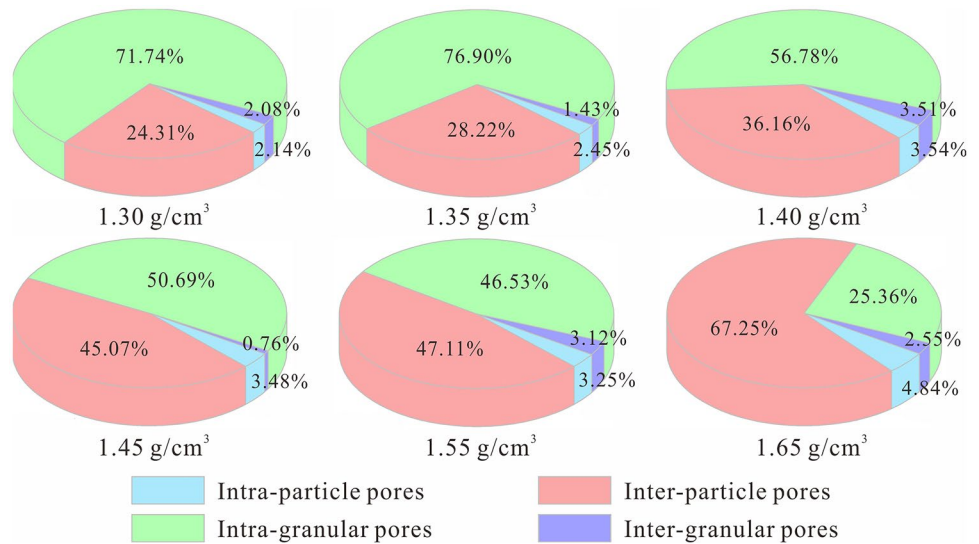
The general trend of the porosity measured by SEM imaging and MIP testing was validated by comparing it with the porosity obtained from Eq. (5), as shown in Fig. 10. In addition, the fitting coefficients between the measured and theoretical porosities were as high as 0.99 and 0.89, indicating that the test results were in good agreement with the theoretical results, thereby supporting the assumption that pores obtained from SEM imaging and MIP testing can represent the variation of pore content in compacted loess. However, theoretical porosities were less than the calculated values.

SEM measured the porosity by visually calculating the pore area ratio of two-dimensional images, but the soil was a three-dimensional structure. Thus, the porosity deviated from the theoretical calculation value because of lacking statistics of three-dimensional parameters. Li and Li (2017) and Li et al. (2019) also have obtained similar findings in the quantitative characterization of the microstructure of loess using the SEM technique and the IPP software, which verified that the results in this study are reasonable. For MIP testing, the theoretical calculation assumed that the pores in

**Table 4** Pore classification results based on MIP test

	Dry density/g·cm <sup>-3</sup>					
	1.30	1.35	1.40	1.45	1.55	1.65
Intra-particle pores	0.008	0.007	0.009	0.007	0.007	0.007
Inter-particle pores	0.094	0.083	0.093	0.096	0.096	0.101
Intra-granular pores	0.276	0.200	0.146	0.108	0.095	0.038
Inter-granular pores	0.008	0.004	0.009	0.002	0.006	0.004
Total pores	0.386	0.295	0.257	0.214	0.205	0.150

**Fig. 9** Ratio of various kinds of pore volumes to the total pore volume



the soil are connected to each other and that mercury only penetrates the connected pores (Giesche 2006; Zhang et al. 2019). The compacted loess contained abundant independent closed pores, resulting in the small test porosity value. Meanwhile, the MIP assumes that the pores are cylindrical; however, there are a lot of bottleneck pores in the compacted soil samples (Zhang et al. 2019). This is one of the reasons for the low test value. Moreover, the measured porosity by SEM or MIP demonstrated a good linear relationship with the correlation coefficient of 0.91 (Fig. 10), also suggesting the rationality of the analysis results. In all, although a certain difference existed between the measured and theoretically calculated porosities, the two methods adequately evaluated the pore distribution characteristics.

As shown in Fig. 11, the pore classification characteristics of compacted loess with different compaction degrees were further compared and evaluated based on SEM and MIP tests. The lower limit of the pore diameter of compacted loess measured by SEM imaging was 0.1 μm; the small test range is a likely factor that made the porosity to be less than the theoretical value. The range of pore diameter measured by MIP was wide, and the lower limit was 6.03 nm. However, because of the “ink-bottle effect” in the mercury injection process, the MIP test overestimated the small pore content and underestimated the large pore content (Giesche 2006; Rabot et al. 2018; Zhang et al. 2015). Therefore, the inter-particle pore content (diameter between 0.014 and 1.8 μm) measured by MIP was higher than the micropore content (diameter < 2 μm) measured by SEM; the influence of compactness

on the latter was weak. Furthermore, according to the SEM quantitative test analysis, increasing the compaction degree of compacted loess mainly increased the pore size change beyond 2 μm, i.e., macropores (diameter > 32 μm) transformed into mesopores (diameter between 8 and 32 μm) and then transformed into small pores (diameter between 2 and 8 μm). Correspondingly, the SEM qualitative analysis results showed that increasing the compactness of compacted loess mainly caused the overhead pores to transform into interlocking pores and then to cemented pores; the transformation was to compress the pore space. The MIP test quantitatively showed that compaction mainly caused the intra-granular pore compression (diameter between 1.8 and 70 μm), transforming larger pores to smaller pores. These qualitative and quantitative variation characteristics of pores imply the potential evolution mechanism of compacted loess with the increase of compaction degree. It is generally summarized that loess particle aggregates were formed through the attraction force after water spraying. Increasing compactness promotes large-scale aggregates to be crushed into small-scale aggregates, filling the pores. When the compactness reaches a certain degree, for example a dry density of 1.65 g/cm³ (corresponding compaction degree of 94.83%), particle aggregates are difficult to be broken, while the flocculation of particles further compresses the pore space and improve the soil compactness. Overall, these three analysis results were consistent, verifying the reliability of SEM and MIP tests. Therefore, the combination of SEM imaging and MIP testing is effective for

**Table 5** Theoretical porosity of compacted loess samples

Dry density/g·cm <sup>-3</sup>	1.30	1.35	1.40	1.45	1.55	1.65
Theoretical porosity/%	52.03	50.18	48.34	46.49	42.80	39.11

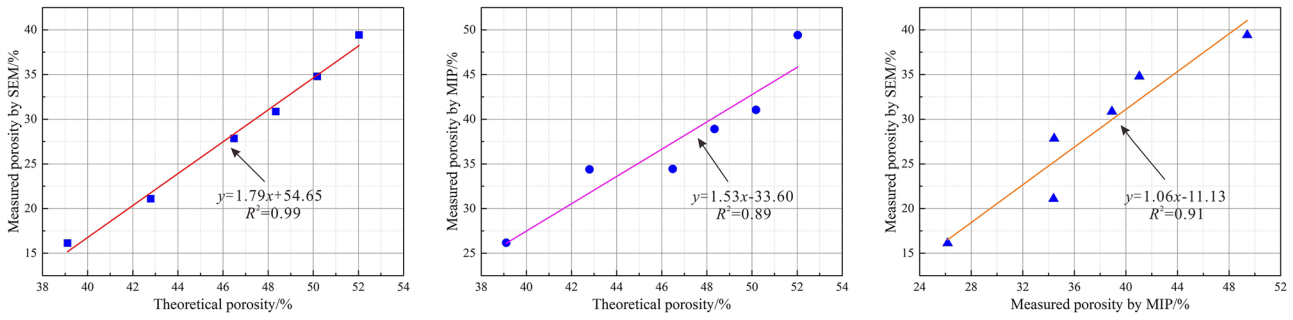


Fig. 10 Relationship between measured and theoretical porosities

complementing their advantages and comprehensively analyzing soil microstructure.

**Engineering implications**

The application of compacted loess as “structure-less reference soil” to the study of structural properties of undisturbed loess, and the corresponding compaction degree is usually less than 80%, which has a theoretical significance in discussing the structure of undisturbed loess while lacking practical guiding significance in the geological engineering

construction of compacted loess (Ma 2017). In this study, as the dry density (compaction degree) increased, the microstructure of compacted loess exhibited an evolution model from an overhead weak cementation structure to an interlocking semi-cementation structure and then to a dispersion-cementation structure. The structure of the 1.30–1.40 g/cm<sup>3</sup> compacted loess was mainly the overhead weak cementation type with weak stability (Fig. 5 and Table 3). According to pore classification of loess and its influence on collapsibility (Lei 1987; Li et al. 2016), the overhead pores including macropores (> 32 μm) and mesopores (8–32 μm) have a significant effect on collapsibility (Table 6). Therefore, these

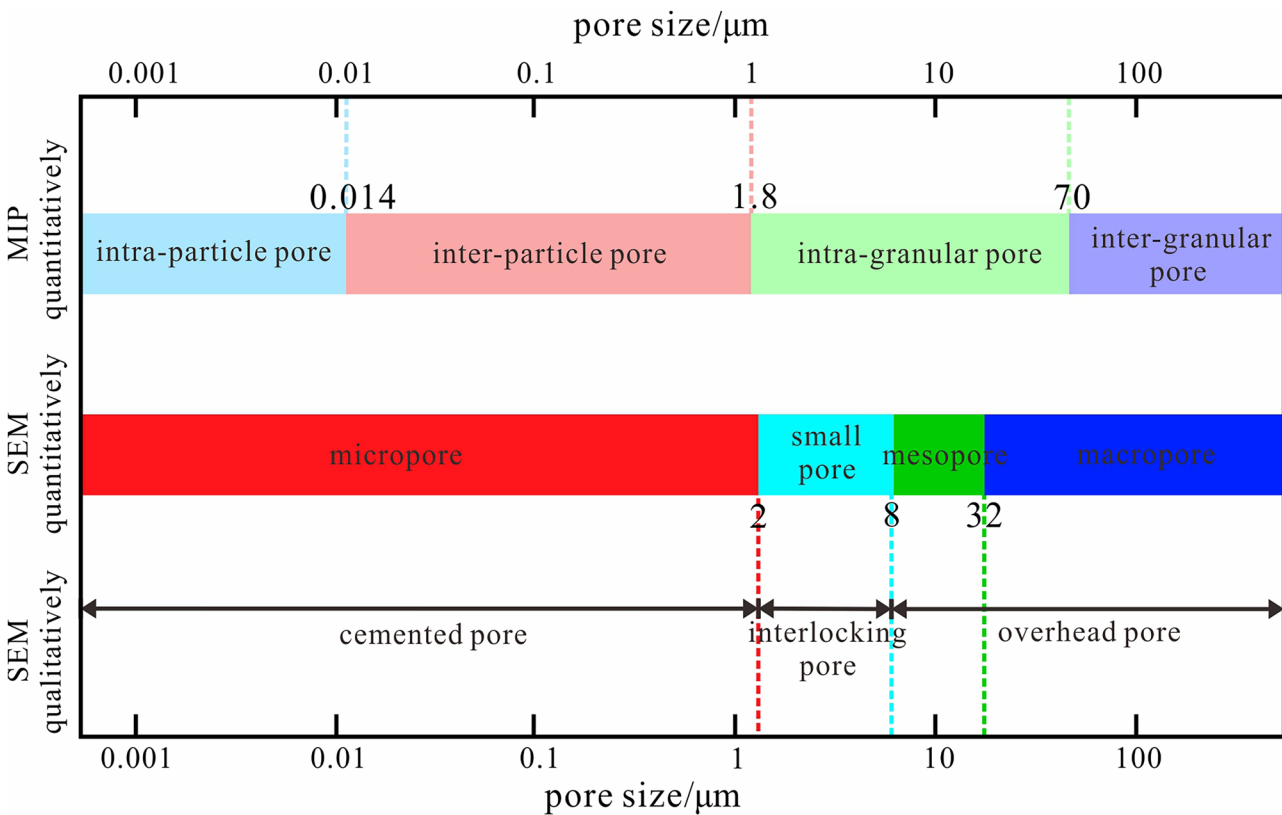


Fig. 11 Comparison of pore sizes in compacted loess characterized based on different methods



**Table 6** Pore classification of loess and its influence on collapsibility (Lei 1987; Li et al. 2016)

Qualitative classification by SEM	Quantitative classification by SEM	Influence on collapsibility
Overhead pores	Macropores(> 32 μm)	Extremely significant
	Mesopores(8–32 μm)	Significant
Interlocking pores	Small pores(2–8 μm)	Not significant
Cemented pores	Micropores(< 2 μm)	Extremely insignificant

small dry density soils have poor structural stability and are prone to collapse in the process of humidification. Their corresponding compaction degrees were 74.71, 77.59, and 80.46%, respectively, which are unsuitable for engineering practice (Ma 2017; Xu et al. 2021c). With an increase in the dry density (compactness) of the samples, such as 1.45–1.65 g/cm<sup>3</sup> (compactness of 83.33–94.83%), the major type of pores gradually changed from interlocking pores to cemented pores (Fig. 5 and Table 3), and small pores and micropores dominated (Figs. 6 and 7), which have no significant impact on loess collapsibility (Table 6). The soil structure of these

dry densities is relatively stable; thus, it is not easy to be damaged and collapsed when encountering water.

Water is the main causative factor for the occurrence of geological disasters in loess. Especially under catastrophic weather such as heavy rainfall, seepage is likely to induce major disaster problems, which has become a basic scientific issue and engineering technology problem that restricts the implementation of our strategy such as “Belt and Road” and “Ecological Protection and High-Quality Development of Yellow River Basin” (Wu et al. 2021). Permeability, as one of the most important hydraulic properties of soil, is used to describe the ease of passage of fluids through porous media, and is widely applied in many disciplines such as hydrogeology and engineering geology (Lu et al. 2021). Thus, understanding the flow behavior of water in soil is of great significance for engineering construction and geological disaster prevention (Cheng et al. 2021; Lee and Ho 2009; Xu et al. 2022b). Taking the Malan loess from Gaozhuang town, Jing Yang county as an example (Fig. 12a), Xu et al. (2021d) found that dry density had a significant impact on the permeability of compacted loess, and reported the change

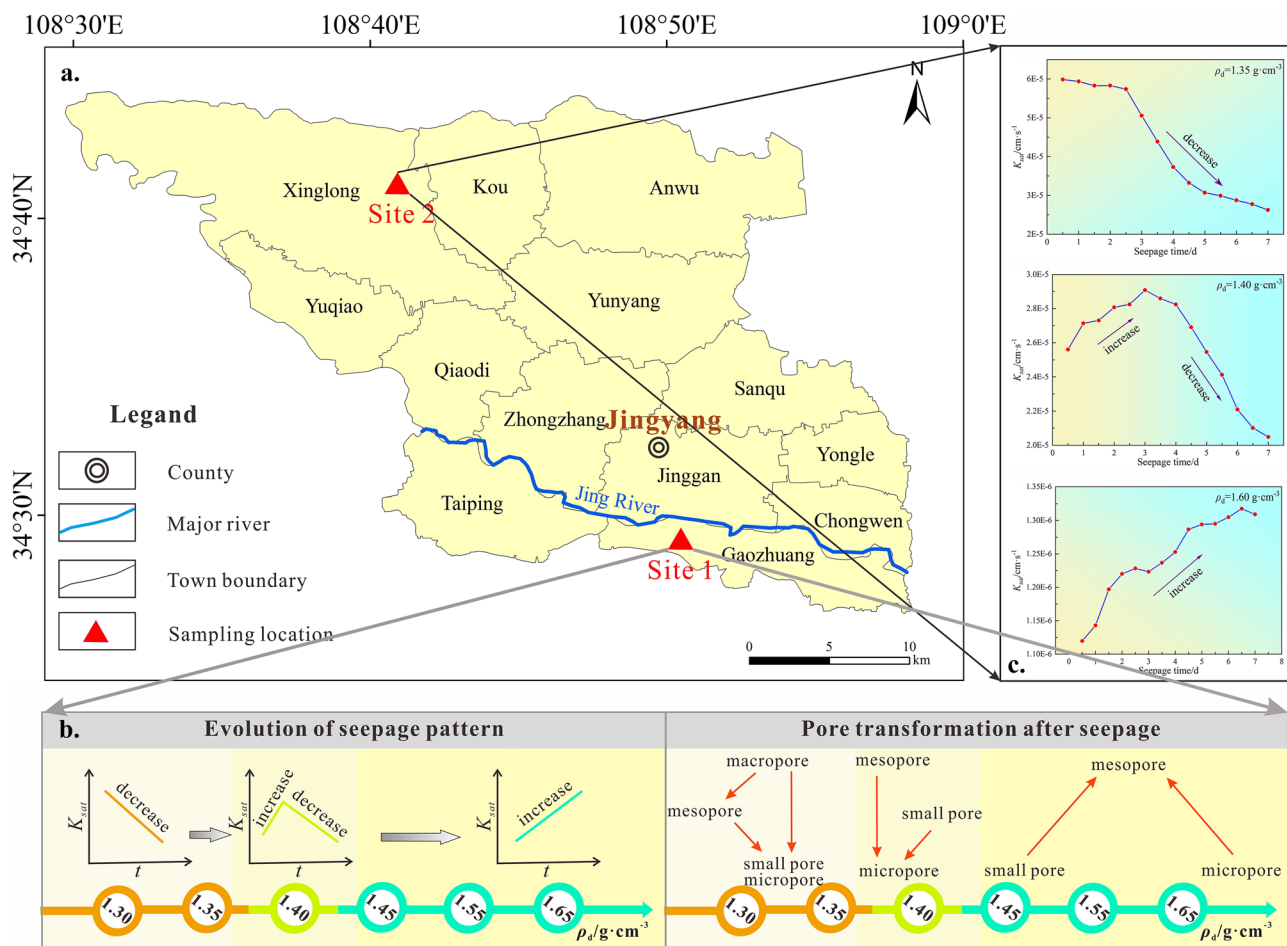


**Fig. 12** Response of the permeability evolution model of compacted loess to dry density (modified from Xu et al. 2021d)

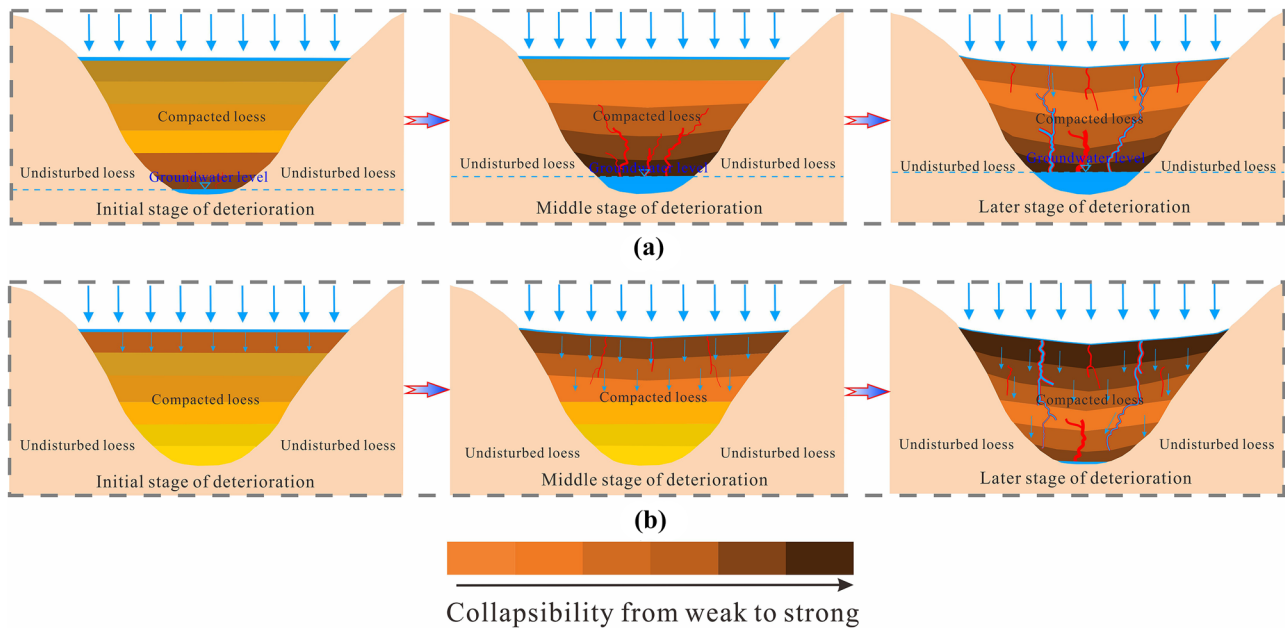


**Fig. 13** Collapsible failure mode of loess filling engineering

mechanism of permeability of compacted loess. The migration effect of fine particles in macropores induces structural collapse, leading to blockage of effective water passage and transformation from larger pores to smaller pores (Xu et al. 2021d). Thus, the permeability of 1.30 and 1.35 g/cm<sup>3</sup> (compactness of 74.71% and 77.59%) compacted loess decreases with time. The compacted loess with dry density of 1.45–1.65 g/cm<sup>3</sup> (compactness of 83.33–94.83%) has a relatively stable structure and no significant or extremely insignificant influence on collapsibility (Table 6). Leaching and dissolution promotes the dissolution of soil components, which enhanced pore development and connectivity. As for 1.40 g/cm<sup>3</sup> (compactness of 80.46%) compacted loess, the dominant mechanism of permeability change is from chemical leaching to collapsibility. The evolution of seepage pattern and the pore transformation after seepage presented in Fig. 12b can explain the above mechanism (Xu et al. 2021d). In addition, the Malan loess in Xinglong town of sampling site 2 was also selected for permeability study, and a similar phenomenon was obtained as that of sampling site 1, which verified the reliability of the research results (Fig. 12c).

Collapsibility and permeability noticeably differed because of the different compaction degrees of filled loess. Also, they have a synergistic effect. When the dry density of compacted loess was small, the soil structure collapsibility was significant while the permeability was weakened during seepage (Xu et al. 2021d). The compacted loess at the lower part of the filling body was infiltrated into an aqueous solution for a long time. The groundwater level increased, resulting in the collapse of the upper part of the filling project,

as shown in Fig. 13a. Soil structure is stable for compacted loess with high compaction degree, such as the top of filling engineering, and the permeability of this type of compacted loess increases with time (Fig. 12). Once leakage occurred, the soil structure deterioration became increasingly noticeable, resulting in the loss of engineering performance, as shown in Fig. 13b. Therefore, an exploration of the evolution characteristics and mechanism of compacted loess microstructure is significant for its engineering properties.

The research on soil structure at microscopic level can provide sufficient basic theoretical support for the portrayal of mechanical behavior at macroscopic level, thus overcoming the phenomenological hypothesis that is detached from the micro-level mechanism. In a word, this study aims to clarify the evolution of the microstructure of compacted loess with compaction and its mechanism in order to provide scientific and reasonable guidance for the engineering construction in loess areas.

## Conclusions

To investigate the evolution characteristics of compacted loess microstructure, samples of compacted loess with six compaction degrees were prepared using a triaxial compaction apparatus. SEM imagery and MIP test were performed on the loess samples to qualitatively and quantitatively determine the formation and evolution mechanism of soil microstructure. The main conclusions are as follows.

As the dry density of the compacted loess increased, the microstructure showed an evolution model from overhead weak cementation structure to interlocking semi-cementation structure and then to dispersion-strong cementation structure. The pore evolution characteristics were mainly from macropores to mesopores and then to small pores, while compaction had a minimal effect on micropores. According to MIP testing, an increase in the compaction degree of compacted loess was followed by a corresponding decrease in the volume content of intra-granular pores, causing the transformation from larger pores to smaller pores. However, the contents of intra-particle, interparticle, and intergranular pores were stable.

The measured porosity demonstrated a good linear relationship with the theoretical porosity. During the microstructure evolution of compacted loess, the variation interval of the dominant pore type (intra-granular pore, diameter between 1.8 and 70  $\mu\text{m}$ ) obtained by the MIP test was consistent with the comprehensive variation interval of macropore (diameter > 32  $\mu\text{m}$ ), mesopore (diameter between 8 and 32  $\mu\text{m}$ ), and small pores (diameter between 2 and 8  $\mu\text{m}$ ) obtained by SEM imagery. The reliability of the evaluation results and the applicability of the method were verified through joint SEM imagery and MIP test. These findings are expected to provide basic data support for loess filling engineering in loess areas.

**Acknowledgements** The authors would like to thank all the reviewers who participated in the review and MJ Editor ([www.mjeditor.com](http://www.mjeditor.com)) for its linguistic assistance during the preparation of this manuscript.

**Funding** The present work was supported by the National Natural Science Foundation of China (Grant Nos. 42202311, 41931285, 42007184, and 41790441), the China Postdoctoral Science Foundation (Grant No. 2022M710480), the Fundamental Research Funds for the Central Universities, CHD (Grant No. 300102292901), the Programme of Introducing Talents of Discipline to Universities (Grant No. B08039), and the Innovation and Entrepreneurship Training Program for College Students (Grant No. S202210710364). Their support is gratefully acknowledged.

## References

- Alabi O (2011) Validity of Darcy's law in laminar regime. *Electron J Geotech Eng* 16:27–40
- Ali A, Biggs AJW, Marchuk A, Bennett JM (2019) Effect of irrigation water pH on saturated hydraulic conductivity and electrokinetic properties of acidic, neutral, and alkaline soils. *Soil Sci Soc Am J* 83(6):1672–1682
- Al-Taie L, Pusch R, Knutsson S (2014) Hydraulic properties of smectite rich clay controlled by hydraulic gradients and filter types. *Appl Clay Sci* 87:73–80
- Assadi-Langroudi A, Ng'ambi S, Smalley I (2018) Loess as a collapsible soil: some basic particle packing aspects. *Quatern Int* 469:20–29
- Assallay AM, Rogers CDF, Smalley IJ (1996) Engineering properties of loess in Libya. *J Arid Environ* 32(4):373–386
- ASTM (2006) Annual book of ASTM standards. ASTM International, West Conshohocken, Pa
- Bourazanis G, Katsileros A, Kosmas C, Kerkides P (2016) The effect of treated municipal wastewater and fresh water on saturated hydraulic conductivity of a clay-loamy soil. *Water Resour Manag* 30(8):2867–2880
- Cheng Q, Tang CS, Xu D, Zeng H, Shi B (2021) Water infiltration in a cracked soil considering effect of drying-wetting cycles. *J Hydrol* 593:125640
- Daniel DE (1994). In: Daniel DE, Trautwein SJ (eds) State-of-the-art: laboratory hydraulic conductivity tests for saturated soils. ASTM International, West Conshohocken, PA, pp 30–78
- Delage P, Lefebvre G (1984) Study of the structure of a sensitive Champlain clay and of its evolution during consolidation. *Can Geotech J* 21(1):21–35
- Derbyshire E (2001) Geological hazards in loess terrain, with particular reference to the loess regions of China. *Earth Sci Rev* 54(1):231–260
- Ge MM, Pineda JA, Sheng DC, Burton GJ, Li N (2021) Microstructural effects on the wetting-induced collapse in compacted loess. *Comput Geotech* 138:104359
- Giesche H (2006) Mercury porosimetry: a general (practical) overview. *Part Part Syst Charact* 23(1):9–19
- Hou K, Qian H, Zhang YT, Zhang QY, Qu WG (2021) New insights into loess formation on the southern margin of the Chinese Loess Plateau. *CATENA* 204:105444
- Hansbo S (2001) Consolidation equation valid for both Darcian and non-Darcian flow. *Geotechnique* 51:51–54
- Jiang M, Zhang F, Hu H, Cui Y, Peng J (2014) Structural characterization of natural loess and remolded loess under triaxial tests. *Eng Geol* 181:249–260
- Jozefaciuk G, Czachor H, Lamorski K, Hajnos M, Swieboda R, Franus W (2015) Effect of humic acids, sesquioxides and silica on the pore system of silt aggregates measured by water vapour desorption, mercury intrusion and microtomography. *Eur J Soil Sci* 66(6):992–1001
- Kloubek J (1981) Hysteresis in porosimetry. *Powder Technol* 29(1):63–73
- Lee KT, Ho JY (2009) Prediction of landslide occurrence based on slope-instability analysis and hydrological model simulation. *J Hydrol* 375(3–4):489–497
- Lei XY (1987) The types of loess pores in China and their relationship with collapsibility. *Sci China B* 17(12):1309–1318 (in Chinese)
- Li G, Wang F, Ma W, Fortier R, Mu Y, Mao Y, Hou X (2018) Variations in strength and deformation of compacted loess exposed to wetting-drying and freeze-thaw cycles. *Cold Reg Sci Technol* 151:159–167
- Li P, Qian H, Wu J (2014) Environment: accelerate research on land creation. *Nature* 510(7503):29–31
- Li P, Vanapalli S, Li T (2016) Review of collapse triggering mechanism of collapsible soils due to wetting. *J Rock Mech Geotech Eng* 8(2):256–274
- Li PF, Sun Q, Geng JS, Yan XS, Tang LY (2022) Radon exhalation from temperature treated loess. *Sci Total Environ* 832:154925
- Li X-A, Li L, Song Y, Hong B, Wang L, Sun J (2019) Characterization of the mechanisms underlying loess collapsibility for land-creation project in Shaanxi Province, China—a study from a micro perspective. *Eng Geol* 249:77–88
- Li XA, Li LC (2017) Quantification of the pore structures of Malan loess and the effects on loess permeability and environmental significance, Shaanxi Province, China: an experimental study. *Environ Earth Sci* 76(15):523
- Li Y (2018) A review of shear and tensile strengths of the Malan loess in China. *Eng Geol* 236:4–10
- Lu Y, Liu SH, Zhang YG, Wang LJ, Li Z (2021) Hydraulic conductivity of gravelly soils with various coarse particle contents subjected to freeze-thaw cycles. *J Hydrol* 598:126302
- Liu Z, Liu F, Ma F, Wang M, Bai X, Zheng Y, Yin H, Zhang G (2015) Collapsibility, composition, and microstructure of loess in China. *Can Geotech J* 53(4):673–686

- Luo H, Wu F, Chang J, Xu J (2018) Microstructural constraints on geotechnical properties of Malan loess: a case study from Zhaojiaan landslide in Shaanxi province, China. *Eng Geol* 236:60–69
- Ma Y (2017) Multiscale research of loess structural behavior. Northwest University, Xi'an (Doctor Thesis)
- Monroy R, Zdravkovic L, Ridley AJG (2010) Microstructural evolution in compacted London clay during wetting and loading. *Géotechnique* 60(2):105–119
- Munoz-Castelblanco JA, Pereira JM, Delage P, Cui YI (2012) The water retention properties of a natural unsaturated loess from northern France. *Geotechnique* 62(2):95–106
- Nan JJ, Peng JB, Zhu FJ, Zhao JY, Leng YQ (2021) Multiscale characteristics of the wetting deformation of Malan loess in the Yan'an area, China. *J Mt Sci* 18(4):1112–1130
- Ng CWW, Sadeghi H, Hossen SKB, Chiu CF, Alonso EE, Baghbanrezvan S (2016) Water retention and volumetric characteristics of intact and re-compacted loess. *Can Geotech J* 53(8):1258–1269
- Pécsi M (1990) Loess is not just the accumulation of dust. *Quatern Int* 7–8:1–21
- Qi S, Vanapalli SK (2015) Hydro-mechanical coupling effect on surficial layer stability of unsaturated expansive soil slopes. *Comput Geotech* 70:68–82
- Rabot E, Wiesmeier M, Schlüter S, Vogel H-J (2018) Soil structure as an indicator of soil functions: a review. *Geoderma* 314:122–137
- Romero E (2013) A microstructural insight into compacted clayey soils and their hydraulic properties. *Eng Geol* 165:3–19
- Shear DL, Olsen HW, Nelson KR (1992) Effects of desiccation on the hydraulic conductivity versus void ratio relationship for a natural clay. Transportation Research Board, USA
- SGTM (2019) Standard for geotechnical testing method (GB/T 50123–2019), National standards of People's Republic of China. China Planning Press, Beijing
- USDA (1951) Soil Survey Manual, U.S. Department of Agriculture (USDA) Agricultural Handbook No. 18. U.S. Government Printing Office, Washington, DC
- Wang H, Qian H, Gao Y (2020a) Non-Darcian flow in loess at low hydraulic gradient. *Eng Geol* 267:105483
- Wang J-D, Li P, Ma Y, Vanapalli SK (2019) Evolution of pore-size distribution of intact loess and remolded loess due to consolidation. *J Soils Sediments* 19(3):1226–1238
- Wang J-J, Qiu Z-F (2017) Anisotropic hydraulic conductivity and critical hydraulic gradient of a crushed sandstone–mudstone particle mixture. *Mar Georesour Geotechnol* 35(1):89–97
- Wang JD, Li P, Ma Y, Vanapalli SK, Wang XG (2020b) Change in pore-size distribution of collapsible loess due to loading and inundating. *Acta Geotech* 15(5):1081–1094
- Wang TM, Wu JG, Kou XJ, Oliver C, Mou P, Ge JP (2010) Ecologically asynchronous agricultural practice erodes sustainability of the Loess Plateau of China. *Ecol Appl* 20(4):1126–1135
- Washburn EW (1921) Note on a method of determining the distribution of pore sizes in a porous material. *Proc Natl Acad Sci USA* 7(4):115
- Wu FC, Liu Y, Zhao XN, Guo ZT et al (2021) Research report on progress strategy of environmental science disciplines. Science Press, Beijing
- Xie W-L, Li P, Zhang M-S, Cheng T-E, Wang Y (2018) Collapse behavior and microstructural evolution of loess soils from the Loess Plateau of China. *J Mt Sci* 15(8):1642–1657
- Xu J, Lan W, Li YF, Wang SH, Cheng WC, Yao XL (2020a) Heat, water and solute transfer in saline loess under uniaxial freezing condition. *Comput Geotech* 118:103319
- Xu P, Lin T, Qian H, Zhang Q (2021a) Anisotropic microstructure of loess-paleosol sequence and its significance for engineering and paleoclimate: a case study from Xiushidu (XSD) profile, southern Chinese Loess Plateau. *Eng Geol* 286:106092
- Xu P, Zhang Q, Qian H, Hou K (2020b) Investigation into microscopic mechanisms of anisotropic saturated permeability of undisturbed Q<sub>2</sub> loess. *Environ Earth Sci* 79(18):412
- Xu PP, Qian H, Zhang QY, Zheng L (2021b) Exploring the saturated permeability of remolded loess under inorganic salt solution seepage. *Eng Geol* 294:106354
- Xu PP, Zhang QY, Qian H, Li MN, Yang FX (2021c) An investigation into the relationship between saturated permeability and microstructure of remolded loess: A case study from Chinese Loess Plateau. *Geoderma* 382:15
- Xu PP, Zhang QY, Qian H, Qu WG, Li MN (2021d) Microstructure and permeability evolution of remolded loess with different dry densities under saturated seepage. *Eng Geol* 282:14
- Xu PP, Zhang QY, Qian H, Yang FX, Zheng L (2021e) Investigating the mechanism of pH effect on saturated permeability of remolded loess. *Eng Geol* 284:105978
- Xu P (2021) Study on water-soil interaction mechanism of permeability change of remolded loess. Chang'an University, Xi'an, China (D.S. Thesis)
- Xu PP, Qian H, Zhang QY, Li WQ, Ren WH (2022a) Investigating saturated hydraulic conductivity of remolded loess subjected to CaCl<sub>2</sub> solution of varying concentrations. *J Hydrol* 612:128135
- Xu PP, Qian H, Zhang QY, Shang JT, Guo YK, Li MN (2022b) Response mechanism of permeability change of remolded loess to seepage parameters. *J Hydrol* 612:128224
- Yan X, Duan Z, Sun Q (2021) Influences of water and salt contents on the thermal conductivity of loess. *Environ Earth Sci* 80(2):1–14
- Zhang T, Ma L, Zhang R, Wang Q, Li J (2019) Analysis for effect of MIP-Based compaction on microstructure of remolded mud stone with “micro-expansion.” *J Eng Geol* 27(04):717–722 (in Chinese)
- Zhang X, Lu T, Lu Y, Lu Y, Li X, Pan W (2018) Characteristics of Malan loess porosity in south Jingyang plateau under scanning electron microscope. *Bull Soil Water Conserv* 38(03):212–216 (in Chinese)
- Zhang X, Qian H, Wu H, Chen J, Qiao L (2016) Multivariate analysis of confined groundwater hydrochemistry of a long-exploited sedimentary basin in Northwest China. *J Chem* 2016:1–15
- Zhang Y, Bing H, Yang CS (2015) Influences of freeze-thaw cycles on mechanical properties of silty clay based on SEM and MIP test. *Chin J Rock Mech Eng* 34(S1):3597–3603
- Zhang Y, Cao W, Wang W, Dong Q (2013) Distribution of groundwater arsenic and hydraulic gradient along the shallow groundwater flow-path in Hetao Plain, northern China. *J Geochem Explor* 135:31–39

Springer Nature or its licensor (e.g. a society or other partner) holds exclusive rights to this article under a publishing agreement with the author(s) or other rightsholder(s); author self-archiving of the accepted manuscript version of this article is solely governed by the terms of such publishing agreement and applicable law.